Research Article

Amjad Ali, Zainab Bukhari, Muhammad Amjad, Sohail Ahmad, Wasim Jamshed*, and Sayed M. El Din

Heat transfer analysis of the MHD stagnation-point flow of third-grade fluid over a porous sheet with thermal radiation effect: An algorithmic approach

https://doi.org/10.1515/phys-2022-0227
received August 14, 2022; accepted January 12, 2023

Abstract: The present article aims to investigate the impacts of the thermal radiation and Lorentz force on the stagnation-point flow of third-grade liquid over a porous stretching sheet with suction. The governing equations are transformed using the similarity transformation. The resulting system of ordinary differential equations is solved using a "so-called" hybrid algorithm based on the finite difference method and the shooting method. The influence of the emerging parameters on the velocity and temperature profiles is analyzed. The results are shown in graphical and tabular forms. For the third-grade liquid flow, the velocity profile shows an inciting trend toward the Hartman number (magnetic parameter). The temperature profile shows a declining trend toward the Prandtl number and suction velocity, whereas an inciting trend towards the radiation parameter.

Keywords: third-grade fluid, heat transfer, thermal radiation, stagnation-point, permeable sheet

*** Corresponding author: Wasim Jamshed,** Department of Mathematics, Capital University of Science & Technology, Islamabad, Pakistan, e-mail: wasiktk@hotmail.com
Amjad Ali, Zainab Bukhari: Centre for Advanced Studies in Pure and Applied Mathematics (CASPAM), Bahauddin Zakariya University, Multan 60800, Pakistan
Muhammad Amjad: Department of Mathematics, COMSATS University Islamabad Vehari Campus, 63100, Islamabad, Pakistan
Sohail Ahmad: Centre for Advanced Studies in Pure and Applied Mathematics (CASPAM), Bahauddin Zakariya University, Multan 60800, Pakistan; Department of Basic Sciences and Humanities, Muhammad Nawaz Sharif University of Engineering and Technology, 60000, Multan, Pakistan
Sayed M. El Din: Center of Research, Faculty of Engineering, Future University in Egypt, New Cairo 11835, Egypt

Nomenclature

B_0	uniform strength
c_p	specific heat
k_1	thermal conductivity
M	magnetic parameter
Nu	Nusselt number
$\tilde{p}$	pressure
Pr	Prandtl number
Rd	radiation parameter
$\mathrm{Re}_{\tilde{x}}$	local Reynolds number
Re	Reynolds number
Sk	skin friction coefficient
T	temperature
T_w	temperature of the sheet
T_∞	temperature away from the sheet
U	characteristic flow velocity
$\tilde{u}$	velocity in $\tilde{x}$-direction
$\tilde{v}$	velocity in $\tilde{y}$-direction
ν	kinematic viscosity
v_w	suction velocity
α_2	material constant
ψ	stream function
θ	temperature profile
ρ	density

1 Introduction

Over recent years, the analysis of nonlinear problems of non-Newtonian fluid flow models has gained popularity due to their industrial applications. Materials such as polymer mixtures, drilling fluids, blood, paints, oils, grease, and many other fluids are categorized as non-Newtonian. They are relevant to a variety of prime engineering and industrial applications. The mathematical

analysis of such models has been challenging for obtaining precise and closed-form solutions. Researchers have been designing algorithms for the investigation of non-Newtonian fluid flow problems with a variety of conditions and contexts. A classical problem of fluid dynamics of stagnation-point flow at a flat surface was investigated using a pioneering work by Hiemenz [1], which was extensively studied by many researchers. Chamkha [2] examined the stagnant-point magnetohydrodynamic (MHD) flow with heat transfer. Wu [3] studied the stagnation-point flow in a permeable space. Teipel [4], Garg and Rajagopal [5,6], and Pakdemirli and Suhubi [7] made efforts for the numerical study of the behavior of viscoelastic stagnation-point flows. Ariel [8,9] used a numerical method for the analysis of the second-grade fluid flow over a porous sheet. Ariel [10] presented a hybrid algorithm for the computations of viscoelastic fluids. Labropulu and Li [11] assumed the slip condition to investigate the second-grade fluid by applying the quasi-linearization method. Abu-Hamdeh *et al.* [12] numerically inquired about the heat transfer performance and fluid flow characteristic of a helical micro double-tube heat exchanger using the finite volume method. More recent investigations regarding thermally developed flows at different temperatures can be studied in the reference articles [13–16].

The researchers extended the literature to discuss the third-grade fluid flow models, which better express the shear thinning and thickening of the viscoelastic fluids than the second-grade fluid flow models. Sajid and Hayat [17] used the homotopy analysis method (HAM) to describe the flow of third-order fluid over an extending surface. Sajid [18] also utilized the HAM to analyze axisymmetric flows for a third-grade liquid. Sahoo [19,20] numerically studied the heat transportation phenomenon in the slip flow of third-grade fluid past a stretchable flat sheet. Hayat *et al.* [21] analyzed mass and heat transport in a third-grade liquid over a stretchable surface with the chemical reaction. Itishree *et al.* [22] examined the unsteady convective flow of third-grade fluid flow through a porous medium. Baoku [23] examined the influence of thermal radiation and suction on the heat transfer and flow characteristics in a third-grade liquid over a vertical porous plate. Hayat *et al.* [24] investigated the transfer of heat in MHD third-grade liquid flow across an extending surface with a heat source and sink. Ramzan *et al.* [25] interpreted the influence of MHD and convective boundary on 2D third-grade liquid flow with the heat flux and chemical reaction. Abbas *et al.* [26] investigated the mass transfer in stagnation-point flow second-grade liquid with a chemical reaction. Zubair *et al.* [27] discussed an application of stagnation-point flow of third-grade liquid with varying thicknesses. Sahoo [28] presented experiments describing third-grade liquids. An account of the history of third-grade liquid was presented by Ikram [29].

An artificial neural network (ANN) was probed by Mishra and Chaudhuri [30] using the Genetic algorithm (GA). The flow was taken between two parallel plates under the influence of uniform heat flux. The ANN model was simplified by the GA, and the results were accomplished. The nonlinear Rosseland approximation to formulate the thermal radiation was considered by Ghasemi and Hatami [31] to interpret the stagnation-point flow over an elongating sheet. They assumed that solar radiation and MHD influenced the flow. Li *et al.* [32,33] measured the convective heat transfer of nanofluid, which potentially is a cost-effective nano-suspension with plausible heat transfer characteristics. CuO–water nano-suspension was prepared, stabilized, and used with the view to improve the thermal conductivity of water and thereby increase the heat transfer coefficient. Literature related to the collective influence of thermal radiation and convection flow of nanofluid due to a stretching cylinder in a porous medium along with viscous dissipation and slip boundary conditions (BCs) were examined by Pandey *et al.* [34–36]. Ali *et al.* [37] investigated the pulsatile flow of viscous incompressible MHD nanofluid in a rectangular channel. Further, several other works investigated the thermal-developed flow of third-grade liquid configured past a permeable stretching/shrinking sheet with additional features at different temperatures [38–43].

We have found from open literature that only a few works express the third-grade boundary layer flow. The present work is an effort towards determining the flow and thermal characteristics of third-grade fluid taking into consideration the simultaneous impacts of thermal radiation and Lorentz force. Flow is assumed to be a stagnation point occurring over a permeable extending surface with suction. Such a specific study was lacking in the literature. Firstly, the differential equations are transformed into dimensionless ordinary differential equations by using appropriate transformations. The system is solved using a "so-called" hybrid algorithm that is based on the finite difference method and the shooting method. A pseudo-code of the algorithms is also presented. The influence of the emerging parameters on the temperature and velocity profiles is analyzed. Furthermore, the effects of the third-grade fluid parameter, Hartman number (magnetic parameter), Prandtl number, and radiation parameter on the heat transfer rate (in terms of the local Nusselt number) are also examined. The results are shown in graphical and tabular forms. The current study can serve as a catalyst for further stretching flow modeling, especially in

polymeric, paper-making, and food-processing applications. We refer the most recent work for further study [44–53]. The rest of the article is structured as follows. In Section 2, the flow equations are presented. In Section 3, the numerical method is presented for the flow problem. Section 4 is about the results and discussions. Section 5 comprises the concluding remarks.

2 Problem formulation

It is assumed that the third-grade fluid flow is two-dimensional, steady, and incompressible which occurs near a stagnation point over a porous stretchable sheet at $\tilde{y} = 0$, as depicted in Figure 1. The porous space is filled with fluid above the sheet, *i.e.*, at $\tilde{y} > 0$. Due to the porosity of the sheet, the suction velocity $v_w = -v_0$, $(v_0 > 0)$ is taken into account. The flow is due to two opposite and equal forces along the stretchable sheet with external flow velocity to the boundary layer, *i.e.*, $U = a\tilde{x}$, where $a > 0$ is a constant, with a fixed origin. The fluid slightly sticks to the sheet, and thus the fluid motion expresses the slip condition. We apply a transverse magnetic field with uniform strength B_0. We define T_w and T_∞ as the temperature of the sheet and the temperature of the immediate fluid, respectively.

The governing model in the Cartesian coordinate system is given by

$$\frac{\partial u}{\partial \tilde{x}} + \frac{\partial v}{\partial \tilde{y}} = 0, \tag{1}$$

$$\begin{aligned} &u\frac{\partial u}{\partial \tilde{x}} + v\frac{\partial u}{\partial \tilde{y}} \\ &= -\frac{1}{\rho}\frac{\partial \hat{p}}{\partial \tilde{x}} + \nu\frac{\partial^2 u}{\partial \tilde{y}^2} + \frac{\alpha_1}{\rho}\left[\nu\frac{\partial^3 u}{\partial \tilde{y}^3}\right. \\ &\quad \left. + \frac{\partial u}{\partial \tilde{x}}\frac{\partial^2 u}{\partial \tilde{y}^2} + u\frac{\partial^3 u}{\partial \tilde{x}\partial \tilde{y}^2} + \frac{\partial u}{\partial \tilde{y}}\frac{\partial^2 v}{\partial \tilde{y}^2}\right] \\ &\quad - \frac{\sigma B_0^2}{\rho}u + \frac{6(\beta_3)}{\rho}\left(\frac{\partial u}{\partial \tilde{y}}\right)^2\left(\frac{\partial^2 u}{\partial \tilde{y}^2}\right), \end{aligned} \tag{2}$$

$$\frac{\partial \hat{p}}{\partial \tilde{y}} = 0, \tag{3}$$

$$\rho c_p\left(u\frac{\partial T}{\partial \tilde{x}} + v\frac{\partial T}{\partial \tilde{y}}\right) = k_1(1 + \mathrm{Rd})\frac{\partial^2 T}{\partial \tilde{y}^2}, \tag{4}$$

where velocity component u is in the $\tilde{x}$-direction while v is in the $\tilde{y}$-direction, ν shows the kinematic viscosity, ρ represents the density of a fluid, c_p represents the specific heat, T gives the temperature, k_1 represents the thermal conductivity, and $\alpha_1 \geq 0$, $\beta_3 \geq 0$ represents the material constants of fluid, Rd represents the thermal radiation

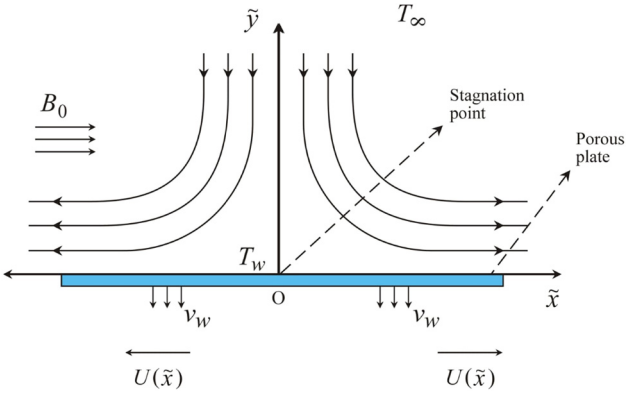

Figure 1: Depiction of the flow geometry.

effect over the sheet, and $\hat{p}$ in Eq. (3) represents the modified pressure, which is defined as follows:

$$\hat{p} = p - (2\alpha_1 + \alpha_2)\left(\frac{\partial u}{\partial \tilde{y}}\right)^2, \tag{5}$$

where α_2 represents material constant. The BCs for this nonlinear system are given as follows:

$$\left.\begin{aligned} u = 0, \quad v_w = -v_0 \quad &\text{at} \quad \tilde{y} = 0 \\ u \to U(\tilde{x}) \quad &\text{as} \quad \tilde{y} \to \infty \end{aligned}\right\}. \tag{6}$$

The relevant temperature conditions are as follows:

$$T(\tilde{x}, 0) = T_w, T(\tilde{x}, \infty) = T_\infty. \tag{7}$$

For simplification of the flow model, the following variables are defined:

$$\left.\begin{aligned} \omega &= \sqrt{\frac{U}{\nu\tilde{x}}}\tilde{y}, \\ \Psi &= \sqrt{U\nu\tilde{x}}\, g(\omega), \\ \theta(\omega) &= \frac{T - T_\infty}{T_w - T_\infty}. \end{aligned}\right\} \tag{8}$$

Further non-dimensional physical quantities which represent the skin friction coefficient and Nusselt number are given below:

$$C_f = \frac{\tau_w}{\frac{1}{2}\rho(ax)^2}, \mathrm{Nu} = \frac{xq_w}{k(T_w - T_\infty)}, \tag{9}$$

where τ_w and q_w are defined as follows:

$$\tau_w = \left[\mu\frac{\partial u}{\partial \tilde{y}} + \alpha_1\left(2\frac{\partial u}{\partial \tilde{x}}\frac{\partial u}{\partial \tilde{y}} + u\frac{\partial^2 u}{\partial \tilde{x}\partial \tilde{y}}\right) + 2\beta\left(\frac{\partial u}{\partial \tilde{y}}\right)^3\right]_{\tilde{y}=0},$$

$$q_w = -k(1 + \mathrm{Rd})\left(\frac{\partial T}{\partial \tilde{y}}\right)_{\tilde{y}=0}.$$

Here Ψ represents the stream function, which satisfies

$$u = \frac{\partial \Psi}{\partial \tilde{y}}, v = -\frac{\partial \Psi}{\partial \tilde{x}}. \tag{10}$$

$\alpha = \frac{a\alpha_1}{\mu}$ and $\beta = \frac{a^2\beta_3}{\mu}$ represents the non-dimensional fluid parameters. $\Pr = \frac{\mu c_p}{k_1}$ represents the Prandtl number, $\mathrm{Re}_{\tilde{x}} = \frac{a\tilde{x}^2}{\nu}$ represents the local Reynolds number, $\mathrm{Rd} = \frac{16\sigma T_\infty^3}{3kk^*}$ represents the radiation parameter, $g_w = \frac{v_0}{\sqrt{a\nu}}$ (with $v_0 > 0$) represents the suction velocity, and $M^2 = \frac{\sigma B_0^2}{\rho a}$ defines the Hartman number M. Note that the parameters α, β, Pr, and n are all positive.

Thus, Eqs. (2) and (4) are transformed into a problem of a system of equations as follows:

$$g''' + gg'' - g'^2 + 1 + M^2(1 - g') + \alpha(2g'g''' - gg^{(\mathrm{iv})} - g''^2) + 6\beta\mathrm{Re}_{\tilde{x}}g''^2g''' = 0, \tag{11}$$

$$(1 + \mathrm{Rd})\theta'' + \mathrm{Pr}g\theta' = 0. \tag{12}$$

Now, the BCs take the following form:

$$\left.\begin{aligned} g(0) = g_w, \quad g'(0) = 0 \\ g'(\infty) = 1, \quad g''(\infty) = 0 \end{aligned}\right\}, \tag{13}$$

$$\theta(0) = 1, \theta(\infty) = 0. \tag{14}$$

The primes in superscript represent the derivatives with respect to ω. Note that $g'(\omega)$ represents the dimensionless fluid velocity. The dimensionless skin friction coefficient C_f, and Nusselt number Nu take the following forms:

$$C_f = \frac{2}{\sqrt{\mathrm{Re}_x}}[g'' + \alpha(g'g'' - gg'') + 2\beta\mathrm{Re}_x g''^3], \tag{15}$$

where $\alpha = \frac{\alpha_1 a}{\mu}$,

$$\mathrm{Nu} = -\sqrt{\mathrm{Re}_x}(1 + \mathrm{Rd})\theta'(0). \tag{16}$$

3 Numerical method with algorithm

For solving the system in Eqs. (11) and (12) subjected to BCs (13) and (14), we obtain a finite domain $[0, 1]$ from the infinite domain $(0, \infty)$ using the transformation

$$\psi = e^{-c\omega}, \tag{17}$$

where c is not a fixed but a changeable parameter. It mainly describes the thickness of the boundary layer for distinct parametric values used in the equation. Further, we transform the dependent variables as follows:

$$G(\omega) = \omega - g(\omega), \theta = \phi, \tag{18}$$

which raises the following boundary value problem

$$G''' + (\omega - G)(G'') - 2G' + G'^2 - M^2G' - \alpha[-2(1 - G')(G''') + (\omega - G)G^{(\mathrm{iv})} - G''^2] + 6\beta\mathrm{Re}_{\tilde{x}}G''^2G''' = 0, \tag{19}$$

$$(1 + \mathrm{Rd})\phi'' + \mathrm{Pr}(\omega - G)\phi' = 0, \tag{20}$$

with BCs

$$\left.\begin{aligned} G(1) = -g_w, \quad G'(1) = 1 \\ G'(0) = 0, \quad G''(0) = 0 \end{aligned}\right\}, \tag{21}$$

$$\phi(1) = 1, \phi(0) = 0. \tag{22}$$

Next we perform the transformation as follows:

$$\tilde{y}_1 = G, \tilde{y}_2 = G', \tilde{y}_3 = G'', \tilde{z} = \phi, \tag{23}$$

and through transformation (17), the system of Eqs. (19) and (20) take the form as given below:

$$\tilde{y}_2 = -c\psi\frac{\mathrm{d}\tilde{y}_1}{\mathrm{d}\psi}, \tag{24}$$

$$\tilde{y}_3 = -c\psi\frac{\mathrm{d}\tilde{y}_2}{\mathrm{d}\psi}, \tag{25}$$

$$\begin{aligned} &c\psi\frac{\mathrm{d}\tilde{y}_3}{\mathrm{d}\psi} + (c^{-1}\ln\psi + \tilde{y}_1)\tilde{y}_3 + 2\tilde{y}_2 - \tilde{y}_2^2 + M^2\tilde{y}_2 \\ &\quad + \alpha\left[2(1 - \tilde{y}_2)c\psi\frac{\mathrm{d}\tilde{y}_3}{\mathrm{d}\psi}\right. \\ &\quad \left.-(c^{-1}\ln\psi + \tilde{y}_1)c^2\psi\frac{\mathrm{d}}{\mathrm{d}\psi}\left(\psi\frac{\mathrm{d}\tilde{y}_3}{\mathrm{d}\psi}\right) - \tilde{y}_3^2\right] \\ &\quad + 6\beta\mathrm{Re}_{\tilde{x}}\tilde{y}_3^2c\psi\frac{\mathrm{d}\tilde{y}_3}{\mathrm{d}\psi} = 0, \end{aligned} \tag{26}$$

$$(1 + \mathrm{Rd})c^2\psi\frac{\mathrm{d}}{\mathrm{d}\psi}\left(\psi\frac{\mathrm{d}\tilde{z}}{\mathrm{d}\psi}\right) + \mathrm{Pr}(c^{-1}\ln\psi + \tilde{y}_1)\left(c\psi\frac{\mathrm{d}\tilde{z}}{\mathrm{d}\psi}\right) = 0. \tag{27}$$

Similarly, the BCs (24) and (25) assume the forms

$$\begin{aligned} &\tilde{y}_2(0) = 0, \quad \tilde{y}_3(0) = 0, \\ &\tilde{y}_1(1) = -g_w, \quad \tilde{y}_2(1) = 1, \end{aligned} \tag{28}$$

$$z(0) = 0, \quad z(1) = 1. \tag{29}$$

The Eqs. (24) and (25) are identically satisfied by the conditions at $\psi = 0$. The mesh on the ψ-axis is formed as follows:

$$\psi = ih \quad \text{where} \quad i = 0, 1, 2, \cdots, N, \tag{30}$$

where N is an integer. The derivatives in the model are discretized using the central differences as follows:

$$\left\{\psi\frac{\mathrm{d}\tilde{y}_3}{\mathrm{d}\psi}\right\}_i = \psi_i\frac{\tilde{y}_3^{i+1} - \tilde{y}_3^{i-1}}{2h}, \tag{31}$$

$$\left\{\psi\frac{\mathrm{d}}{\mathrm{d}\psi}\left(\psi\frac{\mathrm{d}\tilde{y}_3}{\mathrm{d}\psi}\right)\right\}_i = \frac{\psi_i}{h}\left[\psi\frac{\mathrm{d}\tilde{y}_3}{\mathrm{d}\psi}\bigg|_{i+1/2} - \psi\frac{\mathrm{d}^2\tilde{y}_3}{\mathrm{d}\psi^2}\bigg|_{i-1/2}\right], \tag{32}$$

$$= \psi_i\frac{\psi_{i+1/2}(\tilde{y}_3^{i+1} - \tilde{y}_3^{i}) - \psi_{i-1/2}(\tilde{y}_3^{i} - \tilde{y}_3^{i-1})}{h^2}, \tag{33}$$

$$\left\{\frac{\mathrm{d}\tilde{y}_1}{\mathrm{d}\psi}\right\}_i = \psi_{i+1/2}\frac{\tilde{y}_1^{i+1} + \tilde{y}_1^{i}}{h}, \tag{34}$$

Thus, Eqs. (24)–(27) assumes the form as follows:

$$\tilde{y}_1^{i+1} = \tilde{y}_1^{i} - \frac{\tilde{y}_2^{i+1} + \tilde{y}_2^{i}}{c(2i+1)}, \tag{35}$$

$$\begin{aligned}\tilde{y}_3^{i+1} = {} & \left[\frac{ci}{2} - \alpha\left(-ci(1-\tilde{y}_2^{i}) + ci\left(i+\frac{1}{2}\right)(\ln\psi_i + c\tilde{y}_1^{i})\right) + 3ci\beta\,\mathrm{Re}_{\tilde{x}}(\tilde{y}_3^{i})^2\right]^{-1} \\ & \times\left[\frac{ci}{2}\tilde{y}_3^{i-1} - (c^{-1}\ln\psi_i + \tilde{y}_1^{i})\tilde{y}_3^{i} + (\tilde{y}_2^{i})^2 - (2+M^2)\tilde{y}_2^{i} + 3ci\beta\,\mathrm{Re}_{\tilde{x}}(\tilde{y}_3^{i})^2\tilde{y}_3^{i-1}\right. \\ & \left. + \alpha\left(ci(1-\tilde{y}_2^{i})\tilde{y}_3^{i-1} + (\tilde{y}_3^{i})^2\left(+ci(\ln\psi_i + c\tilde{y}_1^{i})\left(-2i\tilde{y}_3^{i} + \left(i-\frac{1}{2}\right)\tilde{y}_3^{i-1}\right)\right)\right)\right],\end{aligned} \tag{36}$$

$$\begin{aligned}\tilde{z}^{i+1} = {} & \left[(1+\mathrm{Rd})c^2i\left(i+\frac{1}{2}\right) + \mathrm{Pr}(\ln\psi + c\tilde{y}_1^{i})\frac{i}{2}\right]^{-1} \\ & \times\left[\mathrm{Pr}(\ln\psi + c\tilde{y}_1^{i})\left(\frac{i}{2}\tilde{z}^{i-1}\right) + (1+\mathrm{Rd})c^2i\left(2i\tilde{z}^{i} - \left(i-\frac{1}{2}\right)\tilde{z}^{i-1}\right)\right],\end{aligned} \tag{37}$$

with respect to BCs:

$$\begin{aligned}\tilde{y}_2^{0} = 0, \quad \tilde{y}_3^{0} = 0, \\ \tilde{y}_1^{N} = -g_w, \quad \tilde{y}_2^{N} = 1.\end{aligned} \tag{38}$$

$$\tilde{z}^{\mathrm{N}} = 1, \tilde{z}^{1} = 0. \tag{39}$$

Thus, the procedure of the hybrid method as adapted from (Ariel [10], Abbas *et al.* [22], and Hayat *et al.* [24]) can be described in the form of pseudocode as below:

INPUTS:
- N, count of mesh nodes
- c, adjustable constant
- α
- β
- M
- Re
- Pr
- Rd
- $\tilde{y}_2^1 = 0$ $\quad \tilde{y}_1^{N+1} = -g_w$
- $\tilde{y}_3^1 = 0$ $\quad \tilde{y}_2^{N+1} = 1$
- $\tilde{z}^1 = 0$ $\quad \tilde{z}^{N+1} = 1$

OUTPUT:
$$\begin{cases}\tilde{Y}_1 = [\tilde{y}_1^1, \quad \tilde{y}_1^2, \cdots, \quad \tilde{y}_1^N, \tilde{y}_1^{N+1}]^T \\ \tilde{Y}_2 = [\tilde{y}_2^1, \quad \tilde{y}_2^2, \cdots, \quad \tilde{y}_2^N, \tilde{y}_2^{N+1}]^T \\ \tilde{Y}_3 = [\tilde{y}_3^1, \quad \tilde{y}_3^2, \cdots, \quad \tilde{y}_3^N, \tilde{y}_3^{N+1}]^T \\ \tilde{Z} = [z^1, \quad z^2, \cdots, \quad z^N, z^{N+1}]^T\end{cases}$$

Step 1: Set $h = \frac{1}{N}$ and $\psi_{i+1} = ih$, for $i = 0, 1, 2, \cdots, N$

Step 2: Construct the values of $\tilde{y}_3^2$ and $\tilde{y}_1^1$ such that $\tilde{y}_2^{N+1} = 1$ and $\tilde{y}_1^{N+1} = -g_w$

Step 3: Construct the values of $\tilde{z}^2$ such that $\tilde{z}^{N+1} = 1$

Step 4: Set $\tilde{y}_2^2 = \tilde{y}_2^1 - \frac{\tilde{y}_3^2 + \tilde{y}_3^1}{3c}$
Set $\tilde{y}_1^2 = \tilde{y}_1^1 - \frac{\tilde{y}_2^2 + \tilde{y}_2^1}{3c}$

Step 5: for $i = 2, 3, 4, \cdots, N$ perform steps 6–9

Step 6: Compute $\tilde{y}_3^{i+1}$ as described in Eq. (37)

Step 7: Compute $\tilde{y}_2^{i+1}$ as described in Eq. (36)

Step 8: Compute $\tilde{y}_1^{i+1}$ as described in Eq. (35)

Step 9: Compute $\tilde{z}^{i+1}$ as described in Eq. (38)

Step 10: Print the outputs.

STOP.

4 Results and discussion

The problem as described in Eqs. (30)–(35) is solved using the algorithm as described in Section 3. The local Reynolds number $\mathrm{Re}_{\tilde{x}}$ is considered as 1 for the study. Some comparisons between the present results and the

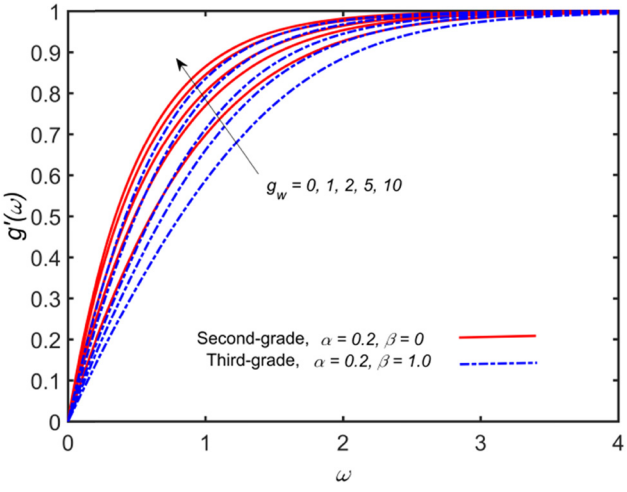

Figure 2: Effects of the suction velocity on the dimensionless fluid velocity.

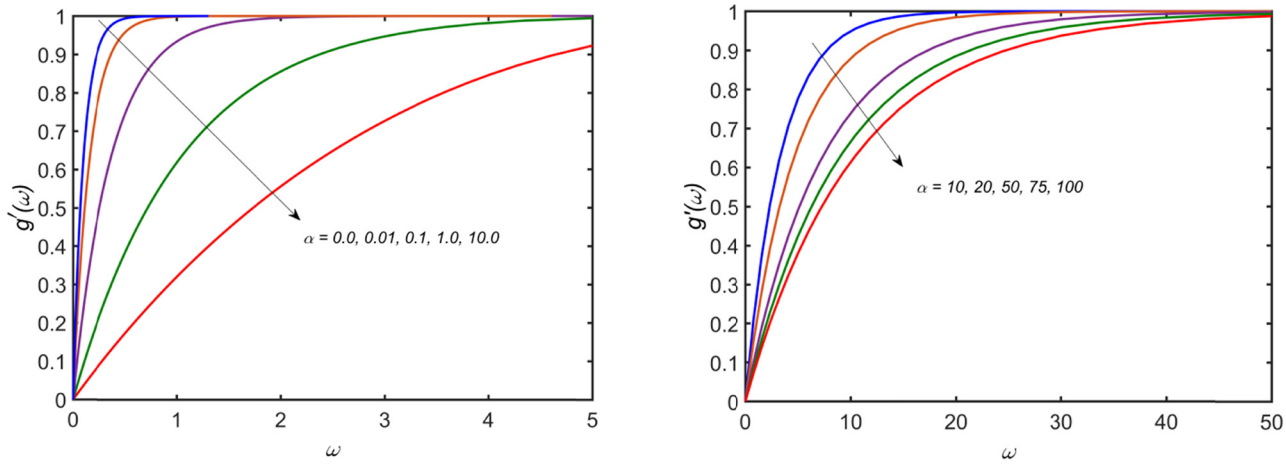

Figure 3: Effects of α on $g'(\omega)$ with $g_w = 10$.

results in the literature are presented to illustrate the validity and accuracy of the solution [25]. The numerical results are presented in Figures 2–9 graphically, which shows the development in the velocity and temperature profiles at various values of the control parameters.

Figure 2 shows the impact of change in g_w, for the second- and third-grade fluids, on $g'(\omega)$. For the case of the second-grade fluid (with $\alpha = 0.2$ and $\beta = 0$), $g'(\omega)$ exhibits slight increments as g_w is increased from 0 to 10. This is because the fluid is of second-grade type (with $\alpha = 0.2$), due to which the suction boundary layer does not appear even for large values of g_w. The plots for the case of the second-grade fluid are found in full agreement with those of previous studies [8] and [22]. For the case of the third-grade fluid (with $\alpha = 0.2$ and $\beta = 1.0$), $g'(\omega)$ exhibits relatively larger increments as g_w is increased from 0 to 10.

Figure 3 shows the effects of α on $g'(\omega)$, taking $g_w = 10$ and $\beta = 0$. In the absence of the viscoelasticity (*i.e.*, $\alpha = 0$), the momentum boundary layer effect is quite apparent because of the suction velocity. For the increasing values of α, the values of $g'(\omega)$ decrease, although the momentum boundary thickness grows with α. The velocity profiles tend to be flattened as α is increased. For higher values of the viscoelastic parameter, no significant variation is found in $g'(\omega)$. The graphs in Figure 3 are in full agreement with the corresponding plots in previous studies [8] and [22].

Figure 4 illustrates the effect of the third-grade fluid parameter β on $g'(\omega)$, when $\alpha = 2$ and $g_w = 1$. $g'(\omega)$ decreases when β increases. It is because of the shear

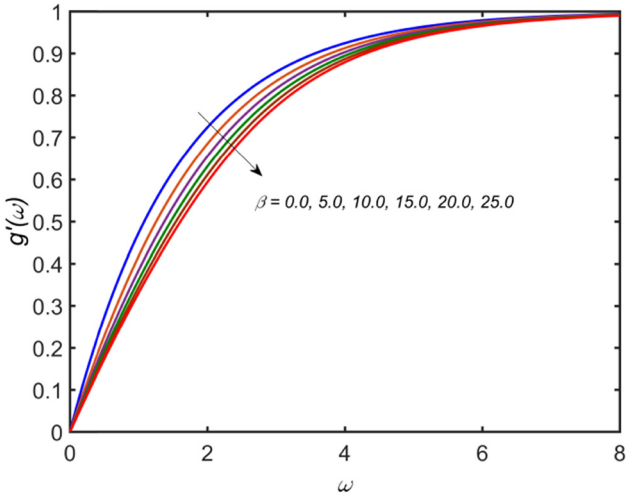

Figure 4: Effect of β on $g'(\omega)$, when $g_w = 1$, $\beta = 1$, and $\alpha = 2$.

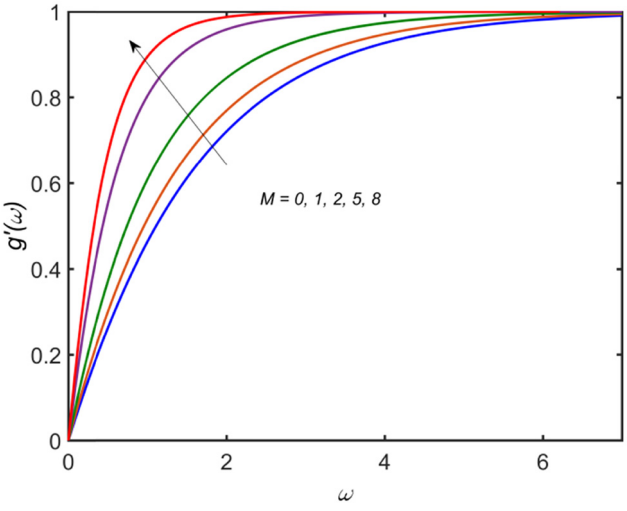

Figure 5: Effect of M on $g'(\omega)$, when $g_w = 1$, $\beta = 1$, and $\alpha = 2$.

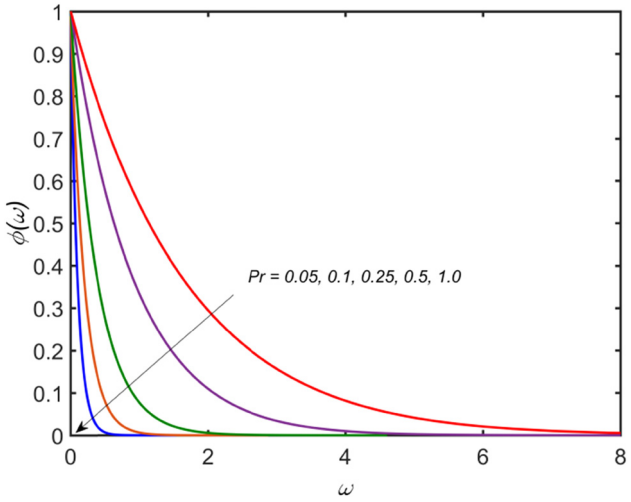

Figure 6: Effect of Pr on $\phi(\omega)$, when $\beta = 1$, $\alpha = 2$, $M = 0.5$ and $g_w = 10$.

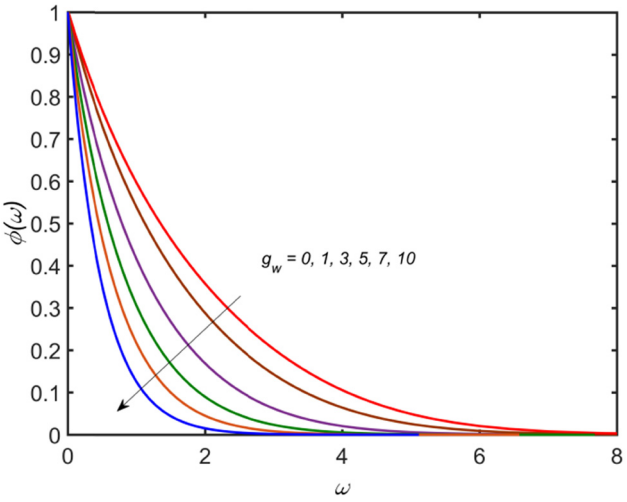

Figure 8: Effect of g_w at $\phi(\omega)$, when $\beta = 1$, $\alpha = 2$, $M = 0.5$ and Pr = 0.2.

thickening effect that grows with β. Also, the third-grade parameter causes an increase in the momentum boundary layer thickness.

Figure 5 shows the effect of Hartman number M on $g'(\omega)$ at different values of ω. The figure illustrates that by decreasing the value of M, the value of velocity field $g'(\omega)$ also decreases. The Lorentz force, which opposes the flow, causes the flow to decelerate more quickly because the Hartmann number directly relates to the Lorentz force. The graphs in Figure 5 are in full agreement with the corresponding plots in the previous study [22] for $M = 0$ and $g_w = 1$.

Figure 6 shows the changes in temperature field $\phi(\omega)$ due to Prandtl number Pr for $\beta = 1$, $\alpha = 2$, $M = 0.5$, and $g_w = 10$. As Pr is a ratio of the thermal diffusivity and momentum diffusivity, hence, temperature field is influenced by the Prandtl number Pr. The values of $\phi(\omega)$ decrease significantly as the Prandtl number is increased. Figure 7 shows the variation in $\phi(\omega)$ due to the radiation Rd when Pr = 0.2. The values of $\phi(\omega)$ increase with the increase in Rd. Figure 8 shows the effects of g_w on $\phi(\omega)$ when Pr = 0.2. The values of $\phi(\omega)$ decrease with the increments in g_w. The velocity of the fluid increases because of suction, which causes a decrease in the temperature.

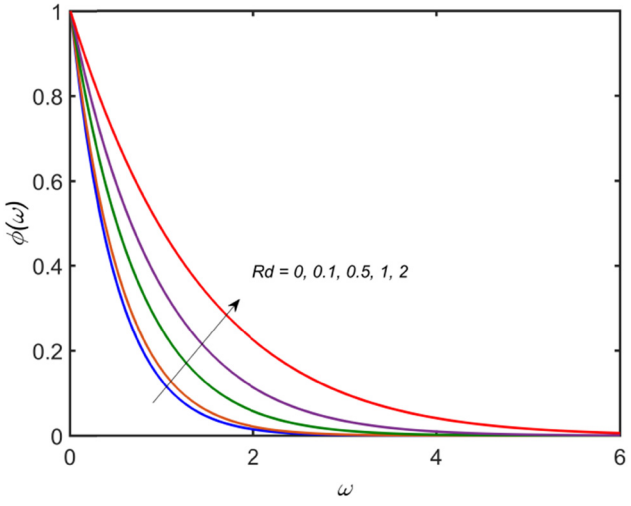

Figure 7: Effect of Rd on $\phi(\omega)$, when $\beta = 1$, $\alpha = 2$, $g_w = 10$, $M = 0.5$ and Pr = 0.2.

Figure 9 shows the impact of β, Pr, and Rd on the important physical quantity, the local rate of heat transfer measured in terms of the local Nusselt number, Nu for $\alpha = 2$, $M = 0.5$, and $g_w = 10$. Nu is observed to be increasing with an increment in β and Rd, whereas it declines when Pr is increased. Since Pr is the ratio of dynamic viscosity to thermal diffusivity, increasing Pr causes the fluid molecules to disperse and lose energy.

Table 1 shows the variation in the values of the temperature gradient at the sheet surface, $\phi'(0)$, for different values of α, β, Pr, and Rd, when $g_w = 5$ and $M = 0.2$. The increments in the values of α, β, and Rd result in the decrement of the temperature gradient (the rate of heat transfer) at the sheet surface, whereas it increases as the value of Pr is increased.

5 Conclusion

In this research, the two-dimensional stagnation-point flow of third-grade liquid over a stretching sheet with

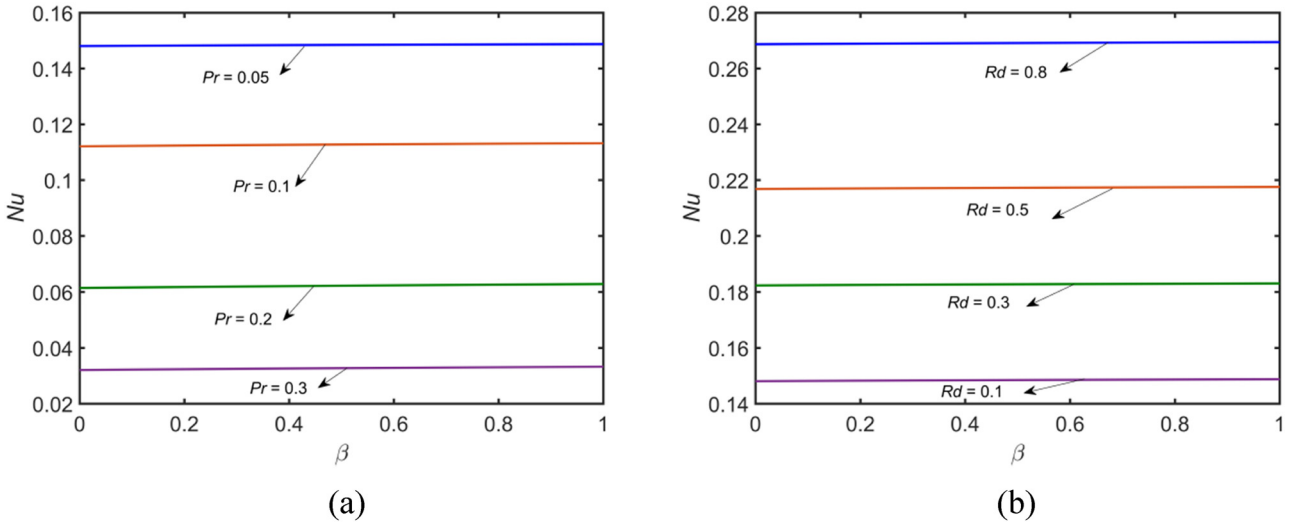

Figure 9: Effect of β on Nu with (a) Pr = 0.05, 0.1, 0.2, and 0.3 and (b) Rd = 0.1, 0.3, 0.5, and 0.8, when $\alpha = 2$, $g_w = 10$, and $M = 0.5$.

uniform suction velocity and thermal radiation is investigated numerically. The governing system of equations is solved by using a hybrid numerical algorithm described in pseudocode form. The impacts of different emerging parameters M, α,β , Pr, and Rd on the velocity $g'(\omega)$ and temperature $\phi(\omega)$ profiles are visualized in graphical and tabular forms. The summary of the impacts is as follows:

- $g'(\omega)$ shows an inciting trend towards the suction velocity g_w. However, $g'(\omega)$ exhibits somewhat higher increments in case of the third-grade fluid than the case of the second-grade fluid with increasing values of g_w.
- In the absence of magnetic field (*i.e.*, $M = 0$), $g'(\omega)$ exhibits a declining trend towards each of the second-grade and the third-grade fluid parameters.
- In the case of third-grade fluid, $g'(\omega)$ shows an inciting trend towards M.
- In the presence of the magnetic field, $\phi(\omega)$ shows a declining trend towards Pr and g_w, whereas an inciting trend towards Rd.
- The values of the temperature gradient at the sheet surface, $\phi'(0)$, decreases for the flow controlling parameters α,β , and Rd, whereas increases for Pr.
- The Nusselt number increases with an increase in β and Rd, while it decreases when Pr is increased.

Table 1: Variation in the temperature gradient at the sheet surface for different values of α, β, Pr, and Rd with $g_w = 5$ and $M = 0.2$

α	β	Pr	Rd	$\phi'(0)$
0.1	1	1	1	2.80197
0.2				2.64761
0.5				2.58806
1.0				2.57900
2.0				2.57660
5.0				2.57588
1	0.1			2.58550
	0.2			2.58468
	0.5			2.58238
	1.0			2.57900
	2.0			2.57344
	5.0			2.56176
2	1	0.2		0.63473
		0.5		1.36135
		1.0		2.57660
		1.5		3.78857
		2.0		5.00131
		1	0.0	5.00131
			0.5	3.38451
			1.0	2.57660
			2.0	1.76740
			5.0	0.95452
			10.0	0.59256

The shooting approach could be applied to a variety of physical and technical challenges in the future [12,54–65].

Funding information: The authors state no funding involved.

Author contributions: All authors have accepted responsibility for the entire content of this manuscript and approved its submission.

Conflict of interest: The authors state no conflict of interest.

Data availability statement: All data generated or analyzed during this study are included in this published article.

References

[1] Hiemenz K. Die Grenzschicht an einem in den gleichförmingen Flussigkeitsstorm eingetauchten graden Kreiszylinder. Ding Polytech J. 1911;326:321–4.

[2] Chamkha AJ. Hydromagnetic plane and axisymmetric flow near a stagnation point with heat transfer. Int Commu Heat Mass Trans. 1998;25:269–78.

[3] Wu Q. Stagnation-point flows in a porous medium. Chem Eng Sci. 2005;60:123–34.

[4] Teipel I. Stagnation point flow of a non-Newtonian second-order fluid. Trans Canad Soc Mech Eng. 1988;12(12):57–61.

[5] Garg VK, Rajagopal KR. Stagnation point flow of a non-Newtonian fluid. Mech Res Comm. 1990;17(6):415–21.

[6] Garg VK, Rajagopal KR. Flow of a non-Newtonian past a wedge. Acta Mech. 1991;88:113–23.

[7] Pakdemirli M, Suhubi ES. Similarity solutions of boundary layer equations for second-order fluid. Int J Eng Sci. 1992;30:611–29.

[8] Ariel PD. A numerical algorithm for computing the stagnation point flow of a second grade fluid with/without suction. J Comp App Math. 1995;59(1):9–24.

[9] Ariel PD. On extra boundary condition in the stagnation point flow of second grade fluid. Int J Eng Sci. 2002;40:145–62.

[10] Ariel PD. A hybrid method for computing the flow of viscoelastic fluids. Int J Num Methods Fl. 2008;14:757–74.

[11] Labropulu F, Li D. Stagnation-point flow of a second grade fluid with slip. Int J Nonlin Mech. 2008;43:941–7.

[12] Abu-Hamdeh NH, Alsulami RA, Rawa MJ, Aljinaidi AA, Alazwari MA, Eltaher MA, et al. A detailed hydrothermal investigation of a helical micro double-tube heat exchanger for a wide range of helix pitch length. Case Stud Ther Eng. 2021;28:101413.

[13] Mahdy A, Ahmed SE. Unsteady MHD convective flow of non-Newtonian casson fluid in the stagnation region of an impulsively rotating sphere. J Aero Eng. 2017;30(5):04017036.

[14] Ahemd SE. Modeling natural convection boundary layer flow of micropolar nanofluid over vertical permeable cone with variable wall temperature. Appl Math Mech. 2017;38(33):1171–80.

[15] Chamka A, El-Aziz MM, Ahmed SE. Effects of thermal stratification on flow and heat transfer due to a stretching cylinder with uniform suction-injection. Int J Energy Tech. 2010;2(4):1–7.

[16] Ahemd SE, Mahdy A. Natural convection flow and heat transfer enhancement of a nanofluid past a truncated cone with magnetic field effect. World J Mech. 2012;2(5):272.

[17] Sajid M, Hayat T. Non-similar series solution for the boundary layer flow of a third order fluid over a stretching sheet. App Math Comp. 2007;189(2):1576–85.

[18] Sajid M, Hayat T, Asghar S. Non similar solution for the axisymmetric flow of a third-grade fluid over a radially stretching sheet. Acta Mech. 2007;189:193–205.

[19] Sahoo B. Flow and heat transfer of a non-Newtonian fluid past a stretching sheet with partial slip. Comm Non-lin Sci Num Simulat. 2010;15:602–12.

[20] Sahoo B, Do Y. Effects of slip on sheet-driven flow and heat transfer of a third grade fluid past a stretching sheet. Int Commun Heat Mass Trans. 2010;37:1064–71.

[21] Hayat T, Mustafa M, Asghar S. Unsteady flow with heat and mass transfer of third grade fluid over a stretching surface in the presence of chemical reaction. Nonlin Anal Real World App. 2010;11:3186–97.

[22] Itishree A, Nayak K, Padhy S. Numerical solution for the flow and heat transfer of a third-grade fluid past a porous vertical plate. Adv Stud Theor Phy. 2012;6:615–24.

[23] Baoku G. Effects of suction and thermal radiation on heat transfer in a third grade fluid over a vertical plate. Phy SciInt J. 2014;4:1293–310.

[24] Hayat T, Shafiq A, Alsaedi A, Asghar S. Effect of inclined magnetic field in flow of third grade fluid with variable thermal conductivity. AIP Adv. 2015;5:087108.

[25] Ramzan M, Bilal M, Chung JD. Effects of MHD homogeneous-heterogeneous reactions on third grade fluid flow with Cattaneo-Christov heat flux. J Mol Liq. 2016;223:1284–90.

[26] Abbas Z, Javed T, Ali N, Sajid MH. Diffusion of chemically reactive species in stagnation-point flow of a third grade fluid: a hybrid numerical method. J App Fluid Mech. 2016;9(1):195–203.

[27] Zubair M, Waqas M, Hayat T, Alsaedi A, Ayub M. Stagnation point flow of third-grade liquid due to variable thickness: A useful application to non-Fourier heat flux approach. Res Phy. 2018;8:1010–6.

[28] Sahoo B. Hiemenz flow and heat transfer of a third grade fluid. Comm Non-lin Sci Num Simulat. 2009;14:811–26.

[29] Ikram H. Heat transfer in a third-grade fluid flow with suction velocity. M.Phil. thesis. Multan: Bahauddin Zakariya University; 2019.

[30] Mishra VK, Chaudhuri S. Genetic algorithm-assisted artificial neural network for retrieval of a parameter in a third grade fluid flow through two parallel and heated plates. Heat Trans. 2020;50:2090–128.

[31] Ghasemi SE, Hatami M. Solar radiation effects on MHD stagnation point flow and heat transfer of a nanofluid over a stretching sheet. Case Stu Ther Eng. 2021;25:100898.

[32] Li Z, Khaled U, Al-Rashed AA, Goodarzi M, Sarafraz M, Meer R. Heat transfer evaluation of a micro heat exchanger cooling with spherical carbon-acetone nanofluid. Int J Heat Mass Trans. 2020;149:119124.

[33] Li Z, Mazinani A, Hayat T, Al-Rashed AA, Alsulami H, Goodarzi M, et al. Transient pool boiling and particulate deposition of copper oxide nano-suspensions. Int J Heat Mass Trans. 2020;155:119743.

[34] Pandey AK, Kumar M. Natural convection and thermal radiation influence on nanofluid flow over a stretching cylinder in a porous medium with viscous dissipation. Alex Eng J. 2017;56(1):55–62.

[35] Pandey AK, Upreti H, Joshi N, Uddin Z. Effect of natural convection on 3D MHD flow of MoS_2–GO/H_2O via porous surface due to multiple slip mechanisms. J Taibah Univ Sci. 2022;16(1):749–62.
[36] Pandey AK, Kumar M. Boundary layer flow and heat transfer analysis on Cu-water nanofluid flow over a stretching cylinder with slip. Alex Eng J. 2017;56(1):55–62.
[37] Ali A, Bukhari Z, Amjad M, Ahmad S, Din E, Tag ES, et al. Newtonian heating effect in pulsating MHD nanofluid flow through a constricted channel: A numerical study. Front Ener Res. 2022;10:1002672.
[38] Naganthran K, Nazar R, Pop I. Unsteady stagnation-point flow and heat transfer of a special third grade fluid past a permeable stretching/shrinking sheet. Sci Rep. 2016;6:25632.
[39] Nazeer M, Ali N, Ahmad F, Latif M. Numerical and perturbation solutions of third-grade fluid in a porous channel: Boundary and thermal slip effects. Pramana. 2020;94:44.
[40] Abdlmalek Z, Khan SU, Waqas H, Nabwey HA, Tlili I. Utilization of second order slip, activation energy and viscous dissipation consequences in thermally developed flow of third grade nanofluid with gyrotactic microorganisms. Symmetry. 2020;12:309.
[41] Li Z, Sarafraz M, Mazinani A, Moria H, Tlili I, Alkanhal TA, et al. Operation analysis, response and performance evaluation of a pulsating heat pipe for low temperature heat recovery. Energy Convers Manage. 2020;222:113230.
[42] Safaei MR, Elkotb MA, Alsharif AM, Mansir IB, Alamri S, Tirth V, et al. An innovative design of a high strength and low weight sudden micro expansion by considering a nanofluid: Electronic cooling application. Case Stud Ther Eng. 2021;28:101637.
[43] Ahmed SE, Oztop HF, Mansour MA, Abu-Hadeh NH. MHD mixed thermo-bioconvection in porous cavity filled by oxytactic microorganisms. Therm Sci. 2016;22:319.
[44] Ragupathi P, Ahammad NA, Wakif A, Shah NA, Jeon Y. Exploration of multiple transfer phenomena within viscous fluid flows over a curved stretching sheet in the co-existence of gyrotactic micro-organisms and tiny particles. Mathematics. 2022;10(21):4133.
[45] Ragupathi P, Ahammad NA, Wakif A, Shah NA. Hydrothermal and mass impacts of azimuthal and transverse components of Lorentz forces on reacting Von Kármán nanofluid flows considering zero mass flux and convective heating conditions. Mathematics. 2022;10:4133.
[46] Shah NA, Wakif A, El-Zahar ER, Ahmad S, Yook SJ. Numerical simulation of a thermally enhanced EMHD flow of a heterogeneous micropolar mixture comprising (60%)-ethylene glycol (EG), (40%)-water (W), and copper oxide nanomaterials (CuO). Case Stud Ther Eng. 2022;35:102046.
[47] Rasool G, Shah NA, El-Zahar ER, Wakif A. Numerical investigation of EMHD nanofluid flows over a convectively heated Riga pattern positioned horizontally in a Darcy-Forchheimer porous medium: application of passive control strategy and generalized transfer laws. Waves Random Complex Media. 2022. doi: 10.1080/17455030.2022.2074571.
[48] Qureshi MZA, Faisal M, Raza Q, Ali B, Botmart T, Shah NA. Morphological nanolayer impact on hybrid nanofluids flow due to dispersion of polymer/CNT matrix nanocomposite material. AIMS Math. 2023;8(1):633–56.
[49] Rauf A, Shah NA, Mushtaq A, Botmart T. Heat transport and magnetohydrodynamic hybrid micropolar ferrofluid flow over a non-linearly stretching sheet. AIMS Math. 2023;8(1):164–93.
[50] Eswaramoorthi S, Loganathan K, Faisal M, Botmart T, Shah NA. Analytical and numerical investigation of Darcy-Forchheimer flow of a nonlinear-radiative non-Newtonian fluid over a Riga plate with entropy optimization. Ain Shams Eng J. 2022;14:101887.
[51] Sajjan K, Shah NA, Ahammad NA, Raju CSK, Kumar MK, Weera W. Nonlinear Boussinesq and Rosseland approximations on 3D flow in an interruption of Ternary nanoparticles with various shapes of densities and conductivity properties. AIMS Math. 2022;7(10):18416–49.
[52] Priyadharshinim P, Archana MV, Ahammad NA, Raju CSK, Yook S-J, Shah NA. Gradient descent machine learning regression for MHD flow: Metallurgy process. Int Comm Heat Mass Trans. 2022;138:106307.
[53] Oreyeni T, Shah NA, Popoola AO, Elzahar ER. The significance of exponential space-based heat generation and variable thermophysical properties on the dynamics of Casson fluid over a stratified surface with nonuniform thickness. Waves in Random and Complex Media. 2022. doi: 10.1080/17455030.2022.2119304.
[54] Ahmadi AA, Arabbeiki M, Ali HM, Goodarzi M, Safaei MR. Configuration and optimization of a minichannel using water–alumina nanofluid by non-dominated sorting genetic algorithm and response surface method. Nanomaterials. 2020;10:901.
[55] Akkoli K, Banapurmath N, Shivashimpi M, Soudagar MEM, Badruddin IA, Alazwari MA, et al. Effect of injection parameters and producer gas derived from redgram stalk on the performance and emission characteristics of a diesel engine. Alexand Eng J. 2021;60:3133–42.
[56] Alazwaria MA, Safaei MR. Combination effect of baffle arrangement and hybrid nanofluid on thermal performance of a shell and tube heat exchanger using 3-D homogeneous mixture model. Mathematics. 2021;9:881.
[57] Ali MS, Anwar Z, Mujtaba M, Soudagar MEM, Badruddin IA, Safaei MR, et al. Two-phase frictional pressure drop with pure refrigerants in vertical mini/micro-channels. Case Stud Ther Eng. 2021;23:100824.
[58] Goodarzi M, Tlili I, Moria H, Alkanhal TA, Ellahi R, Anqi AE, et al. Boiling heat transfer characteristics of graphene oxide nanoplatelets nano-suspensions of water-perfluorohexane (C6F14) and water-n-pentane. Alexand Eng J. 2020;59:4511–21.
[59] Goodarzi M, Tlili I, Moria H, Cardoso E, Alkanhal TA, Anqi AE, et al. Boiling flow of graphene nanoplatelets nano-suspension on a small copper disk. Powder Tech. 2021;377:10–9.
[60] Harari P, Banapurmath N, Yaliwal V, Soudagar MEM, Khan TY, Mujtaba M, et al. Experimental investigation on compression ignition engine powered with pentanol and thevetia peruviana methyl ester under reactivity controlled compression ignition mode of operation. Case Stud Ther Eng. 2021;25:100921.
[61] Homod RZ, Almusaed A, Almssad A, Jaafar MK, Goodarzi M, Sahari KS. Effect of different building envelope materials on thermal comfort and air-conditioning energy savings: A case study in Basra city. Iraq, J EnerStor. 2021;34:101975.
[62] Li Z, Khaled U, Al-Rashed AA, Goodarzi M, Sarafraz M, Meer R. Heat transfer evaluation of a micro heat exchanger cooling with spherical carbon-acetone nanofluid. Int J Heat Mass Trans. 2020;149:119124.

[63] Li Z, Mazinani A, Hayat T, Al-Rashed AA, Alsulami H, Goodarzi M, et al. Transient pool boiling and particulate deposition of copper oxide nano-suspensions. Int J Heat Mass Trans. 2020;155:119743.
[64] Li Z, Sarafraz M, Mazinani A, Moria H, Tlili I, Alkanhal TA, et al. Operation analysis, response and performance evaluation of a pulsating heat pipe for low temperature heat recovery. Ener Conv Manage. 2020;222:113230.
[65] Maddah S, Goodarzi M, Safaei MR. Comparative study of the performance of air and geothermal sources of heat pumps cycle operating with various refrigerants and vapor injection. Alexand Eng J. 2020;59:4037–47.